Title

Changes in Pyruvate Metabolism Detected by Magnetic Resonance Imaging Are Linked to DNA Damage and Serve as a Sensor of Temozolomide Response in Glioblastoma Cells

Journal

Cancer Research, 74(23)

ISSN

0008-5472

Authors

Park, Ilwoo

Mukherjee, Joydeep

Ito, Motokazu

et al.

Publication Date

2014-12-01

DOI

10.1158/0008-5472.can-14-0849

Peer reviewed

Published in final edited form as:
Cancer Res. 2014 December 1; 74(23): 7115–7124. doi:10.1158/0008-5472.CAN-14-0849.

Changes in pyruvate metabolism detected by magnetic resonance imaging are linked to DNA damage and serve as a sensor of temozolomide response in glioblastoma cells

Ilwoo Park[1,*], **Joydeep Mukherjee**[2,4,*], **Motokazu Ito**[2,4], **Myriam M. Chaumeil**[1], **Llewellyn E. Jalbert**[1], **Karin Gaensler**[3], **Sabrina M. Ronen**[1], **Sarah J. Nelson**[1], and **Russell O. Pieper**[2,4]

[1]Department of Radiology and Biomedical Imaging, University of California, San Francisco, San Francisco, California 94158, USA

[2]Department of Neurological Surgery, University of California, San Francisco, San Francisco, California 94158, USA

[3]Department of Hematology/Oncology, University of California, San Francisco, San Francisco, California 94158, USA

[4]Brain Tumor Research Centre, University of California, San Francisco, San Francisco, California 94158, USA

Abstract

Recent findings show that exposure to temozolomide (TMZ), a DNA damaging drug used to treat glioblastoma, can suppress the conversion of pyruvate to lactate. To understand the mechanistic basis for this effect and its potential utility as a TMZ response biomarker, we compared the response of isogenic glioblastoma cell populations differing only in expression of the DNA repair protein MGMT, a TMZ-sensitivity determinant, after exposure to TMZ *in vitro* and *in vivo*. Hyperpolarized [1-$^{(13)}$C]-pyruvate-based magnetic resonance imaging was used to monitor temporal effects on pyruvate metabolism in parallel with DNA damage responses and tumor cell growth. TMZ exposure decreased conversion of pyruvate to lactate only in MGMT-deficient cells. This effect coincided temporally with TMZ-induced increases in levels of the DNA damage response protein pChk1. Changes in pyruvate to lactate conversion triggered by TMZ preceded tumor growth suppression and were not associated with changes in levels of NADH or lactate dehydrogenase activity in tumors. Instead, they were associated with a TMZ-induced decrease in the expression and activity of pyruvate kinase PKM2, a glycolytic enzyme that indirectly controls pyruvate metabolism. PKM2 silencing decreased pyruvate kinase activity, intracellular lactate levels, and conversion of pyruvate to lactate in the same manner as TMZ, and Chk1 silencing blocked the TMZ-induced decrease in PKM2 expression. Overall, our findings showed how TMZ-induced DNA damage is linked through PKM2 to changes in pyruvate metabolism, and how these

Corresponding authors: Russell O. Pieper, HDFCRB, 1450 S. 3rd St, Rm287, San Francisco, CA 94158, 415-502-7132 rpieper@cc.ucsf.edu and Sarah Nelson, Surbeck Laboratory of Advanced Imaging, 1700 4th St., Rm BH-303, San Francisco, San Francisco, CA 94158, (415) 476-6383 sarah.nelson@ucsf.edu.
*I. Park and J. Mukherjee contributed equally to this work.

There are no relationships that could be construed as resulting in an actual, potential, or perceived conflict of interest with regard to this manuscript.

changes can be exploited by magnetic resonance imaging methods as an early sensor of TMZ therapeutic response.

Keywords

pyruvate; metabolism; temozolomide; hyperpolarization; MR imaging

Introduction

Temozolomide (TMZ) is a chemotherapeutic DNA methylating agent useful in the treatment of glioblastoma (GBM)(1,2). DNA O^6-methylguanine (O6MG) lesions created by drug exposure mispair with thymine in the first cycle of DNA replication, leading to activation of the DNA mismatch repair system (3–5). The removal of the thymine opposite O6MG and subsequent reinsertion following repair resynthesis leads to cycles of futile mismatch repair. This in turn ultimately leads to DNA single strand breaks, activation of sensors of DNA damage, the generation of DNA double strand breaks, and delayed cell death by a combination of senescence and mitotic catastrophe (6–10). Because of its limited side effects and proven efficacy, TMZ is a component of the standard therapy for a variety of human brain tumors, and is frequently combined with other experimental agents (2).

Despite its ability to prolong disease-free survival, the response to TMZ-based therapies has proven difficult to monitor in patients. At present, standard imaging techniques are used to monitor the size of contrast-enhancing tumor following initiation of therapy, although for reasons related to difficulties in distinguishing tumor from necrosis and scarring, this approach often proves suboptimal (11, 12). Given that many patients, especially those with low grade gliomas, can remain on TMZ for long periods of time (13), a more effective way to monitor drug efficacy and the early stages of drug failure in real time would allow for better patient stratification as well as for the initiation of alternate approaches in cases of drug failure.

It has been known for over 50 years that tumors metabolically differ from normal cells (14), an observation that has recently been applied to the non-invasive study of tumors by carbon-13 (^{13}C) metabolic imaging. Tumors frequently have high levels of lactate dehydrogenase A (LDH-A), (which preferentially converts pyruvate to lactate) and NADH, the co-factor required for LDH-A activity, both of which may explain the high levels of lactate found in many tumors (15, 16). Changes in the expression of several other tumor-specific metabolic enzymes have also been noted, however, including a shift in expression from pyruvate kinase M1 (which complexes with multiple glycolytic enzymes and facilitates the shunting of pyruvate into the citric acid cycle) to the less active M2 form of the enzyme, which also may contribute to increased pyruvate to lactate conversion (17–19). Based on these observations, the administration of hyperpolarized compounds, most typically pyruvate, to tumor-bearing subjects, followed by the real-time monitoring of conversion of the substrate to various labeled metabolites using ^{13}C 3D magnetic resonance spectroscopic imaging (MRSI) should allow for the localization of malignant tissue (20). Studies along these lines have proven promising, and further work suggested that the approach could also

be used to study drug response because cells undergoing growth arrest or apoptosis convert less hyperpolarized pyruvate to lactate (21–24). More recently, the increased conversion of hyperpolarized pyruvate to lactate was shown to precede the onset of tumor growth, and also was reversed prior to tumor regression, at least in a myc-driven murine model of liver cancer (25). These studies suggest that hyperpolarized ^{13}C MRSI may be a promising way to monitor tumor growth and perhaps tumor drug response.

We previously used hyperpolarized ^{13}C MRSI monitoring to show that human GBM xenografts exhibit an increase in hyperpolarized pyruvate to lactate conversion relative to normal brain (26,27), and that TMZ exposure decreased this conversion in a time frame that preceded histologic and radiographic response (28). Although these findings suggested that pyruvate metabolism might be linked to TMZ response and could serve as a biomarker of TMZ action, it was not clear if the metabolic response was unique to drug sensitive cells, nor was the basis for the metabolic change apparent. To better address these issues, we generated two pairs of isogenic GBM cells which differ only in expression of O6-methylguanine DNA methyltransferase (MGMT), the protein that removes TMZ-induced O6MG lesions before they can mispair and lead to DNA damage, and as such serves as the primary determinant of TMZ sensitivity (29–31). Using these cells we show that the TMZ-induced suppression of the conversion of hyperpolarized pyruvate to lactate is uniquely linked to the TMZ-induced DNA damage response via decreased PKM2 expression and intracellular lactate levels, and as such serves as an early monitor of TMZ response in brain tumor cells.

Materials and Methods

Cell Culture

U87MG human GBM cells, and the same cells expressing MGMT P140K (U87+MGMT), or shRNAs targeting PKM2 (U87+shRNA PKM2) were obtained and cultured as described (31, 32). Suppression of Chk1 protein (>80%) by transfection of siRNA (Santa Cruz Biotechnology) was verified by Western bloting. G55 is a human GBM cell line passaged through nude mice and re-established as a stable xenograft (33), and was provided by the UCSF Brain Tumor Research Center. The G55 cells form invasive intracranial tumors in rodents that are more characteristic of primary human GBM (33). The identity of both cell lines was verified by DNA fingerprinting (Promega Powerplex 16) prior to initiation of the studies.

Intracerebral Tumor Implantation and Imaging Study Scheme

Tumor cells were implanted intracerebrally into male athymic rats (median weight 280g) as described (26–28). Animals received either oral vehicle (Ora-Plus, Paddock Laboratories), oral TMZ (100 mg/kg), intraperitoneal O^6-benzylguanine (BG, 50 mg/kg), or BG followed two hrs later by TMZ when the tumor as monitored by T2-weighted axial images was at least the size of one spectroscopic voxel (approximately 86 mm^3, typically 9–15 days post tumor cell implantation). All animals underwent ^{13}C and ^{1}H imaging prior to treatment (D0, baseline), and one (D1) and/or two (D2) days following treatment.

Polarization Procedure and ^{1}H and ^{13}C MR Imaging

The polarization procedure and *in vivo* imaging have been described previously (17, 24, 25, 27, 34–36). In brief, ^{13}C imaging data were acquired using a compressed sensing or fully sampled ^{13}C 3D MRSI sequence (24,25) at 20 sec from the start of the injection of approximately 2.5 mL hyperpolarized [1-^{13}C]-pyruvate through the tail vein. The compressed sensing data were acquired over 18 seconds, and the fully sampled data over 17 seconds. The injection started ~10 seconds after dissolution and lasted 10 seconds. For tumor volume evaluation, T_1-weighted anatomical images were obtained in the axial plane after the injection of 0.1 mL Gadolinium (Gd)-DTPA (approximately 0.2 mmol/kg) (27).

Data Analysis

The methods for processing ^{13}C MRSI data have been described previously (27, 36, 37). The 3D volume of the contrast enhancing lesion was calculated from the axial T1 post-Gd slices as described (36). At each time point a percent tumor volume change from baseline was calculated, with the last time point being a composite of values derived from multiple paired animals at the termination of the experiment 3–7 days post-TMZ exposure.

Immunohistochemistry

At D1 or D2 post drug treatment, animals were anesthetized (1–2% isoflurane) and perfused with 10% neutral buffered formalin (40 ml). The brains were then removed, fixed in phosphate-buffered 10% formalin, dehydrated by graded ethanols, and embedded in Paraplast Plus wax (McCormick Scientific). Tissue sections were incubated with rabbit monoclonal phospho-Chk1 (Ser345) or polyclonal cleaved caspase-3 (Asp175) antibodies (Cell Signaling Technology) with antigen retrieval. All immunohistochemistry assays were performed on the Benchmark XT (Ventana Medical Systems) using the UltraView detection system.

Perfused cell studies

Approximately 3×10^{7} U87 or U87+shRNA PKM2 cells were grown on Biosilon microcarrier beads (Nunc) for 48 hours, then loaded and analyzed in a 10mm NMR tube connected to an NMR-compatible perfusion system, as previously described (23, 38).

Protein extraction and immunoblot analyses

Whole cell lysates (30 μg protein) were subjected to Western blot analysis using antibodies against Chk1, MGMT, PKM2, and β-actin (all Cell Signaling Technology)(32) with detection by a horse radish peroxidase–conjugated secondary IgG (Santa Cruz Biotechnology) using enhanced chemiluminescence Western blotting detection reagents (Amersham Pharmacia Biotech).

LDH activity and NADH assays

LDH activity and NADH levels were assessed from the D2 resected brains of control and TMZ-treated U87 tumor-bearing rats. Brains were rapidly removed after euthanasia, immediately snap-frozen in liquid N_2, and stored at −80 °C. For LDH activity, K_m and V_{max} values were determined by fitting initial rates of NADH consumption (absorbance at 340

nm) and pyruvate concentrations to a Lineweaver-Burke plot (39). Levels of NADH were determined in tumor extracts using a spectrophotometric enzymatic cycling assay kits (BioVision) according to manufacturer's instructions (40). In brief, tumor tissue was homogenized, centrifuged (14,000g, 5 min) and heated (60 °C, 30 min) to selectively decompose NAD+ in the supernatant. The samples were then diluted 1:10 to fall in the linear range for a standard curve, and mixed with NADH reaction buffer. After 15 min of incubation at room temperature, changes in absorbance at 450 nm caused by the reduction of the reporter molecule thiazolyl blue were measured on a M200 Tecan spectrophotometer (Tecan Group, Männedorf, Switzerland) and compared with a standard curve established using known NADH concentration.

Pyruvate kinase activity and intracellular pyruvate and lactate measurement assay

Intracellular pyruvate kinase activity, as well as concentrations of pyruvate and lactate were measured using pyruvate kinase activity, pyruvate or lactate assay kits, respectively (BioVision).

Results

In vivo biochemical and metabolic response of MGMT-modified GBM cells to TMZ

To first determine if TMZ-induced changes in pyruvate metabolism were related to drug response, two pairs of isogenic cells differing only in MGMT expression were used. TMZ-sensitive, MGMT-deficient GBM cells (U87 cells, and G55 cells pre-incubated with the selective MGMT-depleting agent BG)(41) exhibit increased levels of DNA SSB within one day of an IC_{50} TMZ exposure, accompanied by increased levels of the DNA damage response protein pChk1, and the appearance of DNA DSB beginning two days after TMZ exposure (31). Isogenic TMZ-resistant, MGMT-proficient GBM cells (U87 cells expressing a construct encoding MGMT, and G55 cells) in contrast exhibit no increase in DNA SSB, pChk1, or DSB at one or two days following TMZ exposure (31).

In the first set of studies, control and MGMT-modified U87 GBM cells were intracranially implanted into rats and allowed to form tumors. Animals were then treated with vehicle or TMZ (100 mg/kg) and 24 or 48 hrs later were administered [1-^{13}C]-pyruvate and monitored for conversion of the substrate to lactate by ^{13}C MRSI, for markers of the DNA damage response, and for tumor growth. Non drug-treated cells (U87 vehicle and U87+MGMT vehicle) as well as the TMZ-resistant drug-treated U87+MGMT+TMZ cells (31) exhibited an increase in pyruvate to lactate conversion both one and two days after TMZ treatment (Fig 1A). The TMZ-sensitive drug-treated U87 cells (U87+TMZ), however, exhibited decreased conversion of pyruvate to lactate (compared to pre-treatment D0 tumors) beginning one day after TMZ exposure (Fig 1A). The effect of TMZ on pyruvate to lactate conversion in these cells was consistent temporally with the appearance of cells that stained positively for activated pChk1 (Fig 1B), but preceded the effect of the drug on tumor growth, which was not apparent 1–2 days after TMZ exposure in any cell group, but was apparent in the U87+TMZ cells at the termination of the experiment 3–7 days after TMZ exposure (Fig 1C)(28). These results suggested that TMZ-induced changes in pyruvate to

lactate conversion were related to the formation and/or response to TMZ-induced O6MG, and TMZ response.

To verify and expand on these results, MGMT-proficient, TMZ-resistant G55 GBM cells were intracranially implanted into rats, allowed to form tumors, treated with vehicle, the selective MGMT depleting agent BG, TMZ only, or BG+TMZ, and similarly examined for effects on drug action and metabolic response. As with the tumors generated from the intracranially implanted U87 series of cells, non drug-treated G55 cells (G55+vehicle) as well as the G55 cells incubated with BG (G55+BG) or TMZ alone (G55+TMZ)(31) exhibited an increase in pyruvate to lactate conversion both one and two days after TMZ treatment (Fig 2A). The BG-treated, MGMT-depleted G55 cells (G55+BG+TMZ), however, when exposed to TMZ, exhibited a decreased conversion of pyruvate to lactate (compared to pre-treatment D0 tumors) beginning one day after TMZ exposure (Fig 2A). The effect of TMZ on pyruvate to lactate conversion in these cells appeared co-incident with the appearance of pChk1 staining at one day post TMZ exposure in the TMZ-sensitive G55+BG tumors (Fig 2B), but preceded the effect of the drug on tumor growth, which, consistent with the mechanism of action of the drug, was not apparent 1–2 days after TMZ exposure in any group (Fig 2C), but was apparent in the G55+BG+TMZ tumors, which at the termination of the experiment 3–7 days post-TMZ exposure were 43% smaller than at 2 days, as opposed to G55+TMZ tumors, which nearly doubled in size over the same time period. These results show that the effect of TMZ on pyruvate metabolism is directly related to the absence of MGMT, the generation of O6MG-related DNA damage, and/or the cellular response to these lesions, all of which occur prior to the onset of TMZ-induced growth arrest and cell death.

The TMZ-induced metabolic response is not linked to inhibition of cell growth, induction of apoptosis, changes in NADH levels, or changes in LDH activity

Reductions in the conversion of ^{13}C pyruvate to ^{13}C lactate in *in vivo* imaging studies of drug-treated tumors have been ascribed to a variety of factors including loss of cellularity, apoptosis-induced PARP activation and depletion of NADH levels, decreased LDH-A expression, and loss of LDH activity. In the present study, the decrease in conversion of pyruvate to lactate in response to TMZ occurred within one day of TMZ exposure *in vivo*, long before any changes were noted in tumor growth and long before TMZ-induced O6MG lesions are converted to DNA mismatches and DNA DSB in these cells (31). Similarly, the effects of TMZ on pyruvate to lactate conversion were noted in drug-sensitive cells in the absence of any effect on apoptosis because control and TMZ-treated U87 tumors exhibited equally low levels of caspase-3 staining two days after TMZ exposure (Fig 3A), consistent with the reported inability of these cells to undergo apoptosis in response to TMZ (42). Similarly, although TMZ-sensitive GBM cells could be expected to activate PARP following TMZ exposure in response to TMZ-induced DNA strand breaks (43), no changes in the levels of NADH (Fig 3B) or LDH activity (Fig 3C) were noted in U87 tumors 2 days after TMZ exposure as both the LDH K_m and V_{max} were not significantly different between control and TMZ-treated U87 tumor cells at the time (2 days post TMZ) at which significant differences in pyruvate to lactate conversion were noted (Fig 1A). These results show that the TMZ-induced changes in pyruvate to lactate that are unique to TMZ-sensitive cells occur prior to the onset of growth arrest or cell death, and while related to TMZ-induced DNA

damage and the damage response, appear unrelated to NADH levels and changes in LDH activity.

TMZ alters PKM2 expression and PK activity in a way that contributes to changes in pyruvate metabolism

PKM2 is over-expressed in GBM (32) and in its tetrameric active conformation physically associates with other glycolytic enzymes (hexokinase, glucose 6-phosphate dehydrogenases, glyceraldehyde 3-phosphate dehydrogenase) that are part of the complex that controls the conversion of glucose to pyruvate and the ultimate fate of pyruvate. PKM2 has also been shown to be down-regulated in cells exhibiting alterations in pyruvate to lactate conversion (25), suggesting that its regulation may contribute to the TMZ-induced changes in pyruvate metabolism noted in this study. To address this possibility we monitored the effects of TMZ on PKM2 expression, PK activity, and pyruvate metabolism in TMZ sensitive and TMZ-resistant U87 and G55 cells. Exposure of MGMT-deficient U87 or G55+BG cells, but not MGMT-proficient U87 +MGMT or G55 cells, to TMZ decreased PKM2 expression (Fig 4A) as well as pyruvate kinase activity (Fig 4B) in a time frame (one day following TMZ exposure) consistent with the decrease in pyruvate to lactate conversion in the same cells *in vivo* (Fig 1A, 2A). These results suggest that the DNA-directed effects of TMZ on PKM expression may drive alterations in metabolism. To address this possibility more fully, we used two different shRNAs to suppress PKM2 expression in U87 cells and then monitored the effects on pyruvate metabolism. As shown in Figure 4C, shRNA-mediated suppression of PKM2 expression resulted in a decrease in PK activity similar to that noted following TMZ exposure, as well as decreases in steady-state levels of both pyruvate and lactate in U87 and G55 cells (Fig S3)(32). More importantly, the TMZ-sensitive U87 cells in which PKM2 levels and PK activity were suppressed also exhibited the same significant decrease in the *in vitro* conversion of hyperpolarized [1-^{13}C]-pyruvate to lactate (63.5±4.4% of U87 control, Student's *t*-test $p<0.01$, n=3) (Fig 4D, E), as was noted in TMZ-treated U87 cells. Similarly, *in vitro* levels of intracellular pyruvate and lactate were also significantly reduced in TMZ treated U87 cells, and TMZ +BG-treated, MGMT-depleted G55 cells (Fig S4). These results suggest that the DNA-directed actions of TMZ lead to an early suppression of pyruvate kinase expression, PK activity, and intracellular lactate levels. The decreased intracellular lactate levels in turn are associated with, and may be responsible for (21), the decreased conversion of hyperpolarized pyruvate to lactate noted in TMZ-treated tumors.

pChk1 contributes to the link between TMZ-induced DNA damage and PKM2 expression/ activity

Because TMZ-induced changes in PKM2 expression and pyruvate metabolism were noted within one day of TMZ exposure in MGMT-deficient cells, we considered the possibility that the DNA damage response was linked to these metabolism-related changes. Furthermore, because the onset of Chk1 activation in drug-treated, TMZ-sensitive cells noted here and in previous studies (31) temporally matched that of the changes in metabolism, we examined the specific role of Chk1 in controlling this phenomenon. To do so, U87 and G55 cells were infected with siRNA constructs targeting Chk1, after which effects on PKM2 expression and PK activity were monitored. As shown in Fig 5A, introduction of either of two different Chk1 siRNAs reduced levels of Chk1 by

approximately 80% relative to scramble control cells in both cell lines. Introduction of scramble siRNA into U87 or G55+BG cells did not significantly change PKM2 protein levels while exposure of these cells to an IC_{50} concentration of TMZ significantly decreased levels of PKM2 (Fig 5B and consistent with data in Fig 4A). This degree of TMZ-induced PKM2 suppression was significantly reduced by Chk1 suppression (last column vs adjacent two columns, Fig 5B). Consistent with these observations, exposure of control or scramble siRNA U87 cells, or of G55+BG or G55+BG+scramble siRNA cells to TMZ significantly decreased PK activity, an effect that was also lessened by Chk1 suppression (Fig 5C). These studies show that the Chk1 activation caused by TMZ-induced O6MG damage also contributes to the decreases in PKM2 expression, PK activity, and intracellular lactate levels linked to changes in pyruvate metabolism.

TMZ-induced changes in PKM2 expression and metabolism are a biomarker of response rather than a contributor to TMZ action

Having shown that exposure of TMZ-sensitive, but not TMZ-resistant cells led to decreases in PKM2 expression and PK activity, and that these changes were sufficient to alter pyruvate metabolism, we also considered the possibility that these events were critical downstream components of the cytotoxic action of TMZ in addition to potential biomarkers of TMZ action. To address this possibility we measured the cytotoxic potential of TMZ in drug-sensitive U87 cells and in the same cells in which levels of PKM2 were either genetically suppressed or in which PK activity was increased by virtue of overexpression of the highly active form of PK (PKM1). As shown in Table 1, while the suppression of PKM2 levels in TMZ-sensitive U87 cells that were shown to alter pyruvate metabolism modestly decreased the colony formation ability of the non TMZ-treated cells, it had no effect on TMZ-induced cytotoxicity. Similarly, while over-expression of PKM1 nearly doubled PK activity in U87 cells (32), it also had no significant effect on TMZ-induced suppression of clonagenicity. These results therefore suggest that although TMZ-induced changes in pyruvate metabolism are linked to changes in PKM2 expression, PK activity, and ultimately TMZ-induced DNA adducts, these changes, while separable from the cytotoxic actions of the drug and not per se a contributor to the effects of TMZ on tumor cell clonagenicity, are a marker of TMZ activity (Fig 5D).

Discussion

^{13}C MRSI is capable of monitoring the growth and regression of oncogene-driven tumors (22), and can provide biomarkers of the response of solid tumors to DNA damaging agents and radiation (21). Here we show that ^{13}C MRSI measurements of hyperpolarized pyruvate to lactate conversion, via linkage to regulation of PKM expression and DNA damage, may be useful in measuring the early response of glioma to the commonly used chemotherapeutic methylating agent TMZ.

A variety of studies have used ^{13}C MRSI to examine the linkage between tumor growth, regression, drug response, and pyruvate metabolism, with varying results. Rapid changes in pyruvate metabolism were related to consumption of NADH and subsequent inhibition of LDH-A associated with apoptosis or necrotic cell death (21). Additional studies in

doxorubicin-treated breast adenocarcinomas, however, showed that drug-induced suppression of pyruvate to lactate conversion could be separated from the cell death process, although the metabolic changes were still linked to consumption of NADH and subsequent inhibition of LDH-A associated with drug-DNA damage and PARP activation (44). In the present study, the metabolic effects linked to TMZ sensitivity could be clearly separated from the cell death process and in turn linked to DNA damage, although the exact form of damage that triggers the change in metabolism noted can only be partially determined. The requirement for O6MG lesions, the timing of events, and the data from siRNA suppression studies, however, suggest that Chk1 activation may help link persistent DNA damage to the metabolic changes noted, thus making Chk1 important in both reacting to DNA damage and in providing a non-invasively detectable signal of cellular response.

If O6MG-induced DNA damage and signaling lead to changes in cellular metabolism, how is this accomplished? The present studies suggest that PKM2, a key regulator of cell metabolism known to be over-expressed in GBM may be involved. TMZ-induced DNA damage and Chk1 activation led to decreases in PKM2 levels and activity. Because PKM2 is regulated by a variety of events including phosphorylation, PKM2 may be a target of Chk1 and as such directly linked to the DNA damage response (45–47). Alternatively, the relatively large number of Chk1 substrates may activate pathways that alter PKM2 localization as well as absolute levels in a less direct manner. A number of other kinases including Chk2 are also activated by TMZ in the time frame consistent with the TMZ-induced metabolic changes, and this degree of redundancy may explain the only partial re-aquisition of PKM2 levels and activity following Chk1 knockdown in TMZ-treated cells. The TMZ-induced decrease in PKM2 levels was in turn associated with decreased levels of pyruvate and lactate at least where measured *in vitro*. Given the previously described connection between reduced intracellular lactate levels and decreased conversion of ^{13}Cpyruvate to ^{13}C lactate (21), it seems reasonable that the TMZ-induced decreases in intracellular lactate levels noted here resulted in the decreased pyruvate to lactate conversion in TMZ-treated animals. While direct proof of this linkage would require more complex methods such as diffusion-weighted spectroscopy to measure intracellular lactate levels *in vivo* (48, 49), the present data clearly show that PKM2 plays a key role in linking the DNA damage response to monitorable changes in pyruvate metabolism that in turn relate to drug efficacy.

In addition to identifying the link between TMZ-induced DNA damage and pyruvate metabolism, and defining the mechanism by which this linkage occurs, the present study also has clinical implications. Current monitoring of TMZ action relies on inaccurate and uncertain measures of tumor size gathered over long-periods of time following drug exposure. The studies presented show that at least in a pre-clinical model of GBM, TMZ-induced changes in pyruvate metabolism can provide a much earlier and perhaps more reliable marker of tumor response. Detection of the TMZ-induced changes in metabolism do not rely on measurements of tumor size or contrast enhancement, and in fact appear to precede any drug-induced changes in these parameters. As such this approach may alleviate concerns about inaccuracies of tumor size measurements. In addition, TMZ-induced changes in metabolism are related to the same event (DNA damage) that leads to cell death, but do

not appear to be part of the cell death process. As a result, direct drug-sensitivity information, rather than information indirectly inferred from predictors of DNA damage (such as MGMT promoter methylation)(50), can be obtained rapidly, repeatedly, and in the actual tumor being treated within a day of drug exposure rather than days to weeks later. Clinically, this could allow more rapid decision making and could also limit the exposure of drug-insensitive tumors to mutagens such as TMZ. The latter point could be especially important in low grade astrocytoma, which are frequently treated with TMZ for extended periods of time and which can be driven to progression by TMZ-induced genetic alterations (51). Therefore, although metabolic changes may be driven by events directly linked to cell growth inhibition and cell death, the unique delayed action of TMZ may provide links between the DNA damage response and cell metabolism that can be exploited for improved therapy.

Supplementary Material

Refer to Web version on PubMed Central for supplementary material.

Acknowledgments

Grant Support: NIH grants CA171610, CA097257, and CA118816 (ROP), CA130819 and EB004 (SN), and CA161545, CA172845, CA15491 and EB013598 (SMR).

We thank Lynn DeLosSantos, Dr. Robert Bok, Kristen R. Scott, Pia Eriksson, and Loretta Chan for technical support, and Dr. Tal Raz for statistical analysis.

References

1. Osoba D, Braba M, Yung YKA, Prados MP. Health-related quality of life in patients treated with temozolomide versus procarbazine for recurrent glioblastoma multiforme. J Clin Oncol. 2000; 18:1481–91. [PubMed: 10735896]
2. Johnson DR, O'Neill BP. Glioblastoma survival in the United States before and during the temozolomide era. J Neurooncol. 2011; 106:35–43.
3. Margison GP, Santibanez Koref MF, Povey A. Mechanisms of carcinogenicity/chemotherapy by O6-methylguanine. Mutagenesis. 2002; 17:483–87. [PubMed: 12435845]
4. Karran P, Marinus MG. Mismatch correction at O6-methylguanine residues in E. coli. DNA Nature. 1982; 296:868–69.
5. D'Atri S, Tentori L, Lacal PM, Graziani G, Pagani E, Benincasa E, et al. Involvement of the mismatch repair system in temozolomide-induced apoptosis. J Mol Pharm. 1998; 54:334–41.
6. Hirose Y, Berger MS, Pieper RO. p53 affects both the duration of G2/M arrest and the fate of temozolomide-treated human glioblastoma cells. Cancer Res. 2001; 61:1957–63. [PubMed: 11280752]
7. Quiros S, Roos WP, Kaina B. Processing of O6-methylguanine into DNA double-strand breaks requires two rounds of replication whereas apoptosis is also induced in subsequent cell cycles. Cell Cycle. 2010; 9:168–78. [PubMed: 20016283]
8. Hirose Y, Berger MS, Pieper RO. Abrogation of the Chk1-mediated G2 Checkpoint pathway potentiates Temozolomide-induced toxicity in a p53-independent manner in human glioblastoma cells. Cancer Res. 2001; 61:5843–49. [PubMed: 11479224]
9. Hirose Y, Katayama M, Stokoe D, Haas-Kogan DA, Berger MS, Pieper RO. The p38 mitogen-activated protein kinase pathway links the DNA mismatch repair system to the G2 checkpoint and to resistance to chemotherapeutic DNA-methylating agents. Mol Cell Biol. 2003; 23:8306–15. [PubMed: 14585987]

10. Hirose Y, Katayama M, Mirzoeva OK, Berger MS, Pieper RO. Akt activation suppresses Chk2-mediated, methylating agent–induced G2 arrest and protects from Temozolomide-induced mitotic catastrophe and cellular senescence. Cancer Res. 2005; 65:4861–9. [PubMed: 15930307]
11. Billottet C, Grandage VL, Gale RE, Quattropani A, Rommel C, Vanhaesebroeck B, et al. A selective inhibitor of the p100delta isoform of PI 3-kinase inhibits AML cell proliferation and survival and increases the cytotoxic effects of VP16. Oncogene. 2006; 25:6648–59. [PubMed: 16702948]
12. Venkatash HS, Chaumeil MM, Ward CS, Hass-Kogan DA, James CD, Ronen SM. Reduced phosphocholine and hyperpolarized lactate provide magnetic resonance biomarkers of PI3K/Akt/mTOR inhibition in glioblastoma. Neuro-Onc. 2012; 14:315–325.
13. Friedman HS, Kerby T, Calvert H. Temozolomide and treatment of malignant glioma. Clin Cancer Res. 2000; 6:2585–97. [PubMed: 10914698]
14. Warburg O. On the origin of cancer cells. Science. 1956; 123:309–14. [PubMed: 13298683]
15. Walenta S, Wetterling M, Lehrke M, Schwickert G, Sundfør K, Rofstad EK, et al. High lactate levels predict likelihood of metastases, tumor recurrence, and restricted patient survival in human cervical cancers. Cancer Res. 2000; 60(4):916–21. [PubMed: 10706105]
16. Hirschhaeuser F, Sattler UG, Mueller-Klieser W. Lactate: a metabolic key player in cancer. Cancer Res. 2011; 71:6921–5. [PubMed: 22084445]
17. Guminska M, Ignacak J, Kedryna M, Stachurska B. Tumor-specific pyruvate kinase isoenzyme M2 involved in biochemical strategy of energy generation in neoplastic cells. Acta Biochim Pol. 1997; 44:711–24. [PubMed: 9584851]
18. Kumar Y, Tapuria N, Kimani B, Davidson R. Tumor M2 pyruvate kinase: a gastrointestinal cancer marker. Euro J Gastroenterol Hepatol. 2007; 19:265–276.
19. Christofk HR, Vander Heiden MG, Harris MH, Ramanathan A, Gerszten RE, Wei R, et al. The M2 splice isoform of pyruvate kinase is important for cancer metabolism and tumor growth. Nature. 2008; 452:230–4. [PubMed: 18337823]
20. Brindle K. New approaches for imaging tumor responses to treatment. Nature Rev Cancer. 2008; 8:94–107. [PubMed: 18202697]
21. Day SE, Kettunen MI, Gallagher FA, Hu DE, Lerche M, Wolber J, et al. Detecting tumor response to treatment using hyperpolarized 13C magnetic resonance imaging and spectroscopy. Nature Med. 2007; 13:1382–7. [PubMed: 17965722]
22. Dafni H, Larson PEZ, Hu S, Yoshihara HAI, Ward CS, Venkatesh HS, et al. Hyperpolarized 13C spectroscopic imaging informs on hypoxia-inducible factor-1 and myc activity downstream of platelet-derived growth factor receptor. Cancer Res. 2009; 70:7400–10. [PubMed: 20858719]
23. Ward CS, Venkatesh HS, Chaumeil MM, Brandes AH, VanCriekinge M, Dafni H, et al. Noninvasive detection of target modulation following phosphatidylinositol 3-kinase inhibition using hyperpolarized 13C magnetic resonance spectroscopy. Cancer Res. 2010:1296–305. [PubMed: 20145128]
24. Chaumeil MM, Ozawa T, Park IW, Scotta K, James CD, Nelson SJ, et al. Hyperpolarized 13C MR spectroscopic imaging can be used to monitor Everolimus treatment in vivo in an orthotopic rodent model of glioblastoma. Neuroimage Volume. 2012; 59:193–201.
25. Hu S, Balakrishnan A, Bok RA, Anderton B, Larson PEZ, Nelson SJ, et al. 13C-pyruvate imaging reveals alterations in glycolysis that precede c-myc-induced tumor formation and regression. Cell Metab. 2011; 14:131–42. [PubMed: 21723511]
26. Park I, Larson P, Zierhut ML, Hu S, Bok R, Ozawa T, et al. Hyperpolarized 13C MR metabolic imaging: application to brain tumors. Neuro Oncol. 2010; 12(2):133–44. [PubMed: 20150380]
27. Park I, Hu S, Bok R, Ozawa T, Ito M, Mukherjee J, et al. Evaluation of heterogeneous metabolic profile in an orthotopic human glioblastoma xenograft model using compressed sensing hyperpolarized 3D 13C magnetic resonance spectroscopic imaging. Magn Reson Med. 2013; 70:33–39. [PubMed: 22851374]
28. Park I, Bok R, Ozawa T, Phillips JJ, James CD, Vigneron DB, et al. Detection of early response to temozolomide treatment in brain tumors using hyperpolarized 13C MR metabolic imaging. J Magn Reson Imaging. 2011; 33:1284–90. [PubMed: 21590996]

29. Pegg AE, Wiest L, Foote RS, Mitra S, Perry W. Purification and properties of O6-methylguanine-DNA transmethylase from rat liver. J Biol Chem. 1983; 258:2327–33. [PubMed: 6822564]
30. Friedman HS, Johnson SP, Dong Q, Schold SC, Rasheed BKA, Bigner SH, et al. Methylator resistance mediated by mismatch repair deficiency in a glioblastoma multiforme xenograft. Cancer Res. 1997; 57:2933–36. [PubMed: 9230204]
31. Ito M, Ohba S, Gaensler K, Ronen SM, Mukherjee J, Pieper RO. Early chk1 phosphorylation is driven by Temozolomide-induced, DNA double strand break- and mismatch repair-independent DNA damage. PLoS One. 2013; 8(5):e62351. [PubMed: 23667469]
32. Mukherjee J, Phillips JJ, Zheng S, Wiencke J, Ronen SM, Pieper RO. Pyruvate kinase M2 expression, but not pyruvate kinase activity, is up-regulated in a grade-specific manner in human glioma. PLoS One. 2013; 8(2):e57610. [PubMed: 23451252]
33. Kunkel P, Ulbricht U, Bohlen P, Brockmann MA, Fillbrandt R, Stavrou D, et al. Inhibition of glioma angiogenesis and growth in vivo by systemic treatment with a monoclonal antibody against vascular endothelial growth factor receptor-21. Cancer Res. 2001; 61:6624–28. [PubMed: 11559524]
34. Ardenkjaer-Larsen JH, Fridlund B, Gram A, Hansson G, Hansson L, Lerche MH, et al. Increase in signal-to-noise ratio of > 10,000 times in liquid-state NMR. Proc Natl Acad Sci USA. 2003; 100:10158–63. [PubMed: 12930897]
35. Derby K, Tropp J, Hawryszko C. Design and evaluation of a novel dual-tuned resonator for spectroscopic imaging. J Magn Reson. 1990; 86:645–51.
36. Nelson SJ. Analysis of volume MRI and MR spectroscopic imaging data for the evaluation of patients with brain tumors. Magn Reson Med. 2001; 46:228–39. [PubMed: 11477625]
37. Cunningham CH, Vigneron DB, Chen AP, Xu D, Nelson SJ, Hurd RE, et al. Design of flyback echo-planar readout gradients for magnetic resonance spectroscopic imaging. Magn Reson Med. 2005; 54:1286–89. [PubMed: 16187273]
38. Brandes AH, Ward CS, Ronen SM. 17-allyamino-17-demethoxygeldanamycin treatment results in a magnetic resonance spectroscopy-detectable elevation in choline-containing metabolites associated with increased expression of choline transporter SLC44A1 and phospholipase A2. Breast Cancer Res. 2010; 12(5):R84. [PubMed: 20946630]
39. Vassault, A. Lactate dehydrogenase. UV-method with pyruvate and NADH. In: Bergmeyer, HU., editor. Methods of enzymatic analysis. Vol. 3. Weinheim: Verlag Chemie; 1983. p. 118-26.
40. Bernofsky C, Swan M. An improved cycling assay for nicotinamide adenine dinucleotide. Anal Biochem. 1973; 53:452–8. [PubMed: 4351948]
41. Dolan ME, Pegg AE. O6-benzylguanine and its role in chemotherapy. Clin Cancer Res. 1997; 3:837–47. [PubMed: 9815757]
42. Hirose Y, Berger M, Pieper RO. p53 effects both the duration of G2/M arrest and the fate of temozolomide-treated human glioblastoma cells. Cancer Res. 2001; 61:1957–63. [PubMed: 11280752]
43. Langelier M-F, Planck JL, Roy S, Pascal JM. Structural basis for DNA damage–dependent poly(ADP-ribosyl)ation by human PARP-1. Science. 2012; 336:728–32. [PubMed: 22582261]
44. Witney TH, Kettunen MI, Hu D-E, Gallagher FA, Bohndiek SE, Napolitano F, et al. Detecting treatment response in a model of human breast adenocarcinoma using hyperpolarised [1-13C]pyruvate and [1,4-13C2]fumarate. Br J Cancer. 2010; 103:1400–06. [PubMed: 20924379]
45. Yang W, Lu Z. Regulation and function of pyruvate kinase M2 in cancer. Cancer Lett. 2013; 339 (2):153–8. [PubMed: 23791887]
46. Yang W, Xia Y, Hawke D, Li X, Liang J, Xing D, et al. PKM2 phosphorylates histone H3 and promotes gene transcription and tumorigenesis. Cell. 2012; 150:685–96. [PubMed: 22901803]
47. Shimada M, Niida H, Zineldeen DH, Tagami H, Tanaka M, Saito H, Nakanishi M. Chk1 is a histone H3 threonine 11 kinase that regulates DNA damage-induced transcriptional repression. Cell. 2008; 132:221–32. [PubMed: 18243098]
48. Schilling F, Düwel S, Köllisch U, Durst M, Schulte RF, Glaser SJ, et al. Diffusion of hyperpolarized (13) C-metabolites in tumor cell spheroids using real-time NMR spectroscopy. NMR Biomed. 2013; 26:557–68. [PubMed: 23233311]

49. Pfeuffer J, Lin JC, Delabarre L, Ugurbil K, Garwood M. Detection of intracellular lactate with localized diffusion {1H-13C}-spectroscopy in rat glioma *in vivo*. J Magn Reson. 2005; 177:129–38. [PubMed: 16111904]

50. Hegi ME, Diserens A-C, Godard S, Dietrich P-Y, Regli L, Ostermann S, et al. Clinical trial substantiates the predictive value of O-6-methylguanine-DNA methyltransferase promoter methylation in glioblastoma patients treated with temozolomide. Clin Cancer Res. 2004; 10:1871–4. [PubMed: 15041700]

51. Johnson BE, Mazor T, Hong C, Barnes M, Aihara K, McLean CY, et al. Mutational analysis reveals the origin and therapy-driven evolution of recurrent glioma. Science. 2014; 343:189–93. [PubMed: 24336570]

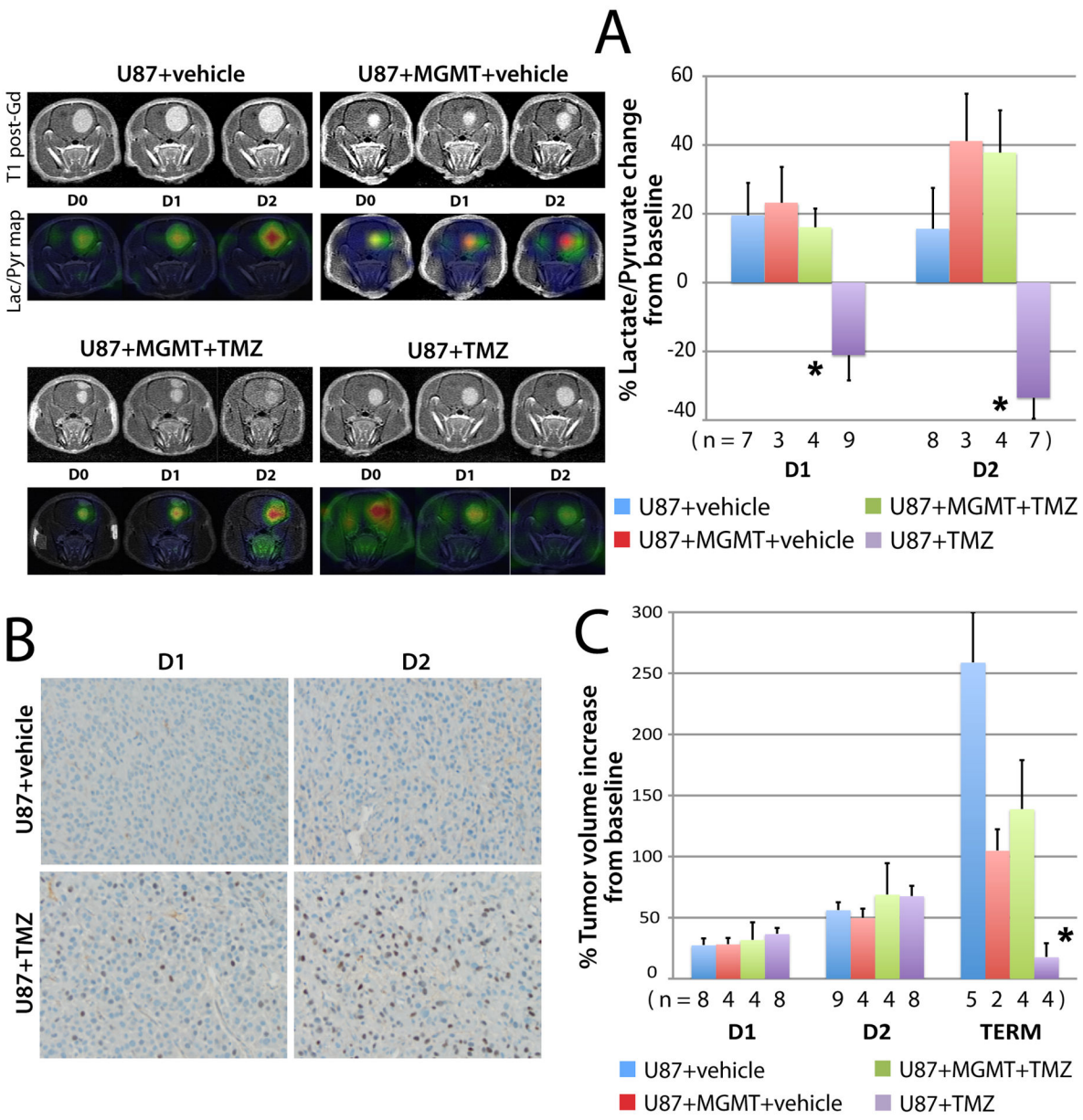

Figure 1. TMZ-induced changes in hyperpolarized ^{13}C pyruvate metabolism precede MGMT-regulated drug response in a U87 GBM human orthotopic xenograft model

(A, left panel) Representative hyperpolarized ^{13}C MRSI data shows T1 post-Gd images and Lac/Pyr overlay map of tumor-bearing animals (U87 or U87+MGMT) at D0, D1 and D2 following TMZ (100 mg/kg) treatment. (A, right panel) Quantitation of the change in lactate/pyruvate ratio from the data in the left panel. (B) The TMZ-induced change in pyruvate metabolism coincided with an increase in phospho-Chk1 staining (Chk1 activation) in the drug-sensitive U87 tumors (panel B, 200x magnification), but preceded drug response which was not apparent at D1 or D2 post TMZ exposure but was apparent in the U87+TMZ group at the termination of the experiment 3–7 days post-TMZ exposure (panel C). The numbers below the x-axis of the graphs in Figure 1A and 1C indicate the numbers of

animals for each group. The ^{13}C spectra at baseline, D1 and D2 post TMZ exposure for panel A are provided in Supplementary Figure 1. *, $p < .05$.

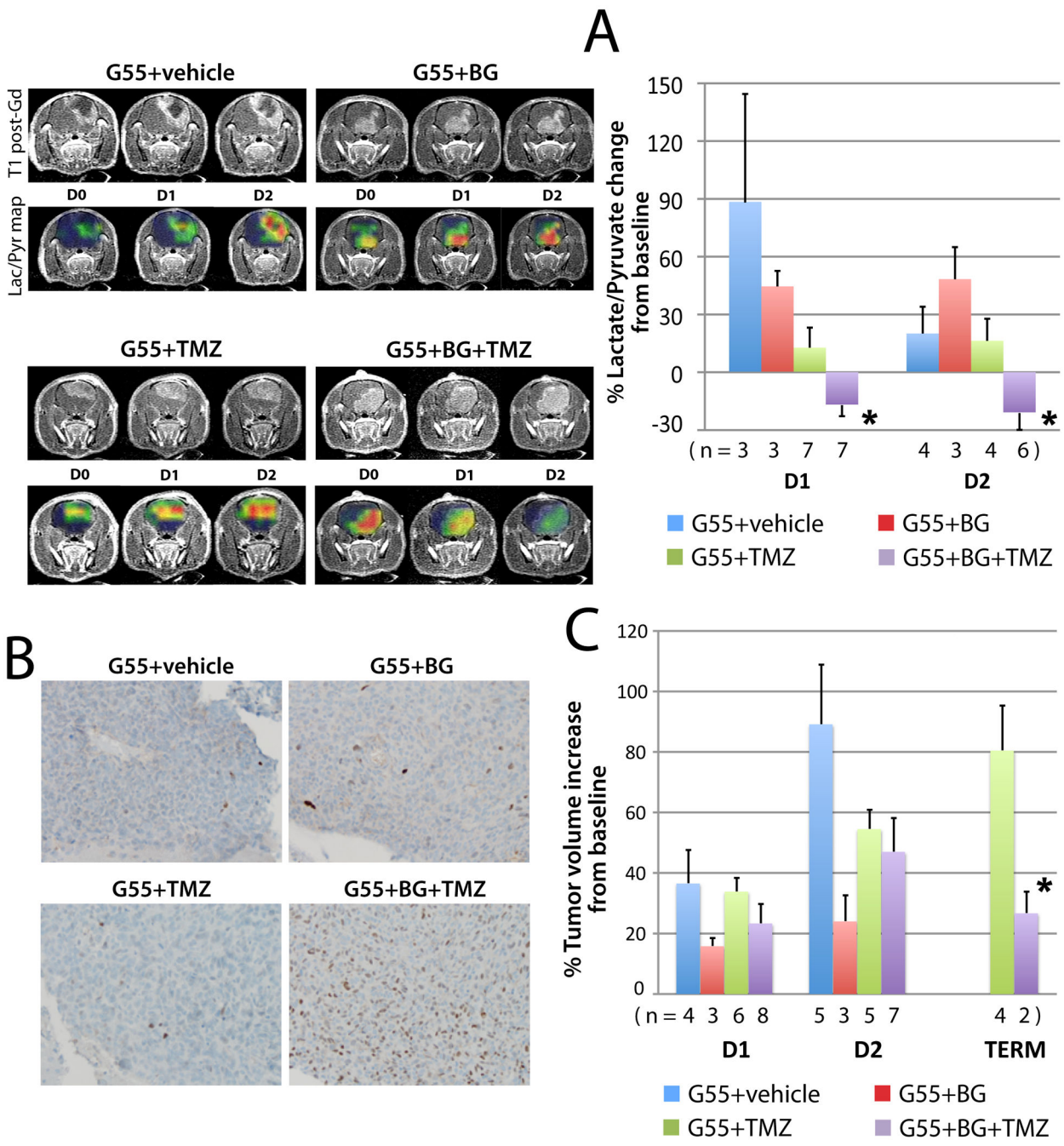

Figure 2. TMZ-induced changes in hyperpolarized ^{13}C pyruvate metabolism precede MGMT-regulated drug response in a G55 GBM human orthotopic xenograft model

(A, left panel) Representative hyperpolarized ^{13}C MRSI data shows T1 post-Gd images and Lac/Pyr overlay map of G55 tumor-bearing animals at D0, D1 and D2 (left panel in A) following vehicle, BG, TMZ (100 mg/kg), or BG+TMZ treatment. The MGMT-deficient, TMZ-treated group (G55+BG+TMZ) exhibited a decrease in pyruvate to lactate metabolism beginning at D1 while all the other groups exhibited increased conversion of pyruvate to lactate (A, right panel). The effect of TMZ on ^{13}C metabolism in the MGMT-depleted, drug-treated tumors (G55+BG+TMZ) coincided with the appearance of pChk1 staining at

one day post TMZ exposure (panel B, 200x magnification), but preceded drug response which was not apparent at D1 or D2 post TMZ exposure but was apparent in the G55+BG +TMZ group at the termination of the experiment 3–7 days post-TMZ exposure (panel C). The numbers below the x-axis of the graphs in Figure 2A and 2C indicate the numbers of animals for each group. The ^{13}C spectra at baseline, D1 and D2 post TMZ exposure for panel A are provided in Supplementary Figure 2. *, $p < .05$.

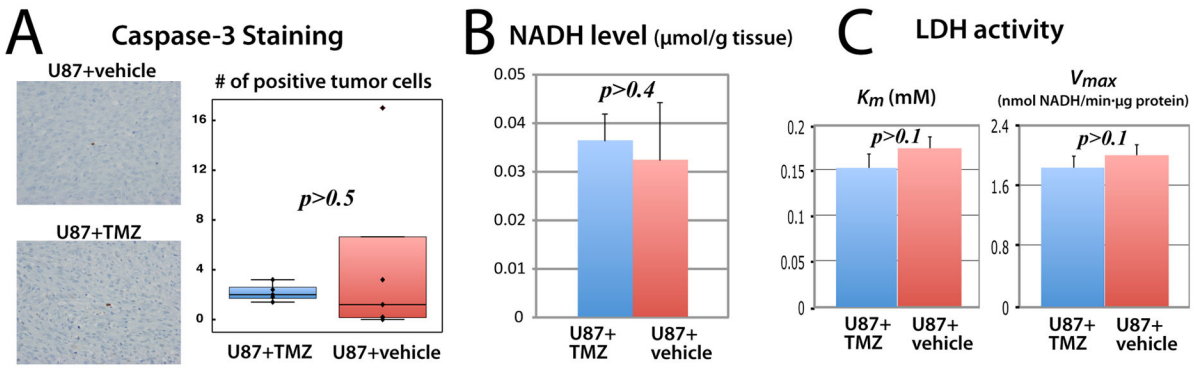

Figure 3. TMZ-induced metabolic response is not related to induction of apoptosis, changes in NADH levels, or changes in LDH activity

TMZ-treated or vehicle-treated animals with MGMT-deficient U87 tumors were euthanized at two days post the initiation of treatment and their brain analyzed for caspase-3 staining (A), NADH level (B), and LDH activity assay (C). N=8 for U87+TMZ and N=7 for U87+vehivle.

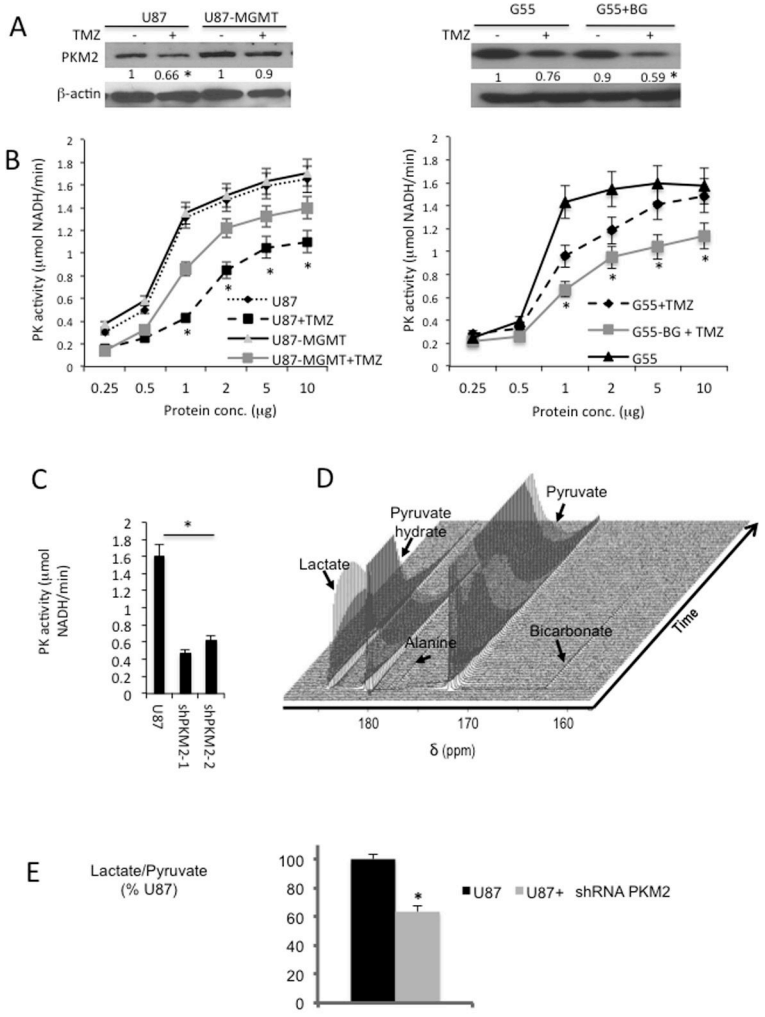

Figure 4. TMZ alters PKM2 expression and PK activity in a way that contributes to changes in pyruvate metabolism

An IC_{50} TMZ exposure (100 μM, 3 hrs) significantly decreased PKM2 protein expression (A) and pyruvate kinase activity (B)(*, p< .05.) in TMZ-sensitive U87 (left panels) and G55+BG (right panels) cells, but not in TMZ-resistant (U87+MGMT or G55) cells. shRNA-mediated suppression of PKM2 expression in U87 cells also caused a decreased in pyruvate kinase activity (C) (*, p< .05). Hyperpolarized [1-^{13}C] lactate production detected in U87 cells following injection of hyperpolarized [1-^{13}C] pyruvate (D). TMZ-sensitive U87 cells with the suppressed levels of PKM2 and pyruvate kinase activity (U87+shRNA PKM2) exhibited decreased conversion of ^{13}C pyruvate to lactate (E) (*, p<0.001).

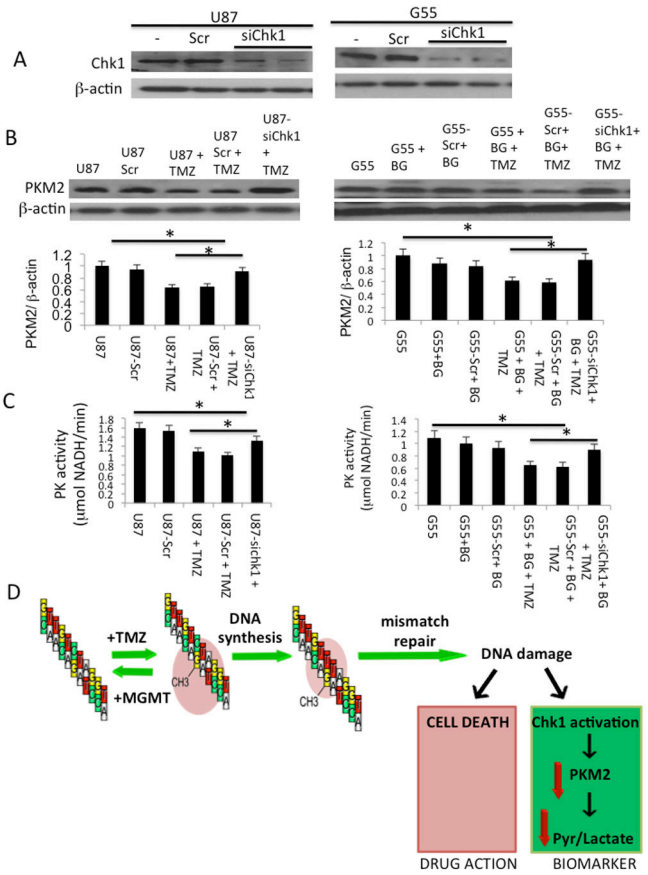

Figure 5. The DNA damage response is linked to PKM2 expression and pyruvate kinase activity

Introduction of siRNAs targeting Chk1 decreased levels of Chk1 protein in U87 and G55 cells (A). PKM2 protein expression (B) and pyruvate kinase activity (C) were significantly decreased 2 days following an IC_{50} TMZ exposure (100 μM, 3 hrs) in TMZ-sensitive U87 control and scramble siRNA cells (left panels), and G55+BG plus scramble siRNA cells (right panels), an effect that was significantly reduced by introduction of Chk1 siRNA into U87 cells and G55 +BG cells. N=3. *, p< .05. Schematic representation of the data (D).

Table 1

Effect of PKM2 knockdown on TMZ sensitivity.

Cell group	Colony number (% control)
U87 control	100
U87 + shRNA PKM2	68 ± 7
U87 + PKM1	65 ± 5
U87+ 100 μM TMZ	3 ± 1
U87+ shRNA PKM2+ 100 μM TMZ	4 ± 2
U87 + PKM1 + 100 μM TMZ	2 ± 1